

# Directional spectra observations of seafloor microseisms from an ocean-bottom seismometer array

Dean Goodman, Tokuo Yamamoto, Mark Trevorrow, Chuck Abbott, Altan Turgut, Mohsen Badiy, and Koichi Ando  
*Geo-Acoustics Laboratory, Rosenstiel School of Marine and Atmospheric Science, University of Miami, 4600 Rickenbacker Causeway, Miami, Florida 33149*

(Received 22 February 1989; accepted for publication 24 July 1989)

Observations of the directional spectra of seabed motion in shallow water were conducted off the New Jersey coast during the summer of 1987. Using a six-point ocean-bottom seismometer array, each instrument supporting a pressure transducer, and two horizontal and vertical accelerometers, measurements of gravity and seismic waves across the ULF/VLF band were collected in 12.5 m of water. Array dimensions were tuned particularly for directional spectra observations of short-period seafloor microseisms. Directional spectra analysis indicates that in the short-period microseismic band, 1.5–2.5 s, motion of the seafloor is primarily a result of slow seismic waves traveling at apparent velocities near 200 m/s. These propagation velocities for the microseismic band in shallow water are an order of magnitude less than microseismic velocities from similar studies on land. Contemporaneous measurements of the directional spectra of long-period ocean gravity waves, 15–85 s, show an eastern direction of origin; short-period ocean gravity waves, 5–9 s, measured using particle motion analysis, are from the south. The direction of propagation of the microseisms, found from the maximum response of the array, is shown to be approximately N150E—a direction midway between long- and short-period ocean-wave propagation directions. Correlation of particle motion and directional spectra analysis indicates that microseisms have retrograde motion. These results suggest that the microseisms are most likely Scholte interface waves.

PACS numbers: 43.30.Nb, 43.30.Ma, 43.40.Ph

## INTRODUCTION

Our understanding of the generation of seafloor microseisms has been advanced by several early classical works on the subject. Longuet-Higgins's<sup>1</sup> theoretical treatment suggests that microseisms develop as a result of ocean gravity waves of similar period traveling in opposite directions. The interference of these waves creates a seafloor pressure fluctuation that is twice the frequency of the dominant gravity wave. Hasselmann<sup>2</sup> provides a statistical treatment for the generation of microseisms using spectral transfer functions. The earliest studies of background noise attribute microseisms to breaking waves, particularly in coastal regions or a result of atmospheric waves and storms (Goerke and Woodward<sup>3</sup>; Sorrells<sup>4,5</sup>). Gutenberg<sup>6</sup> and Ewing and Press,<sup>7</sup> however, found no correlation between microbaroms and microseismic spectra. Considerable effort by Haubrich *et al.*<sup>8</sup> to measure microseisms on land have shown some results consistent with the "frequency doubling effect" described by Longuet-Higgins.<sup>1</sup> Kibblewhite and Ewans<sup>9</sup> have observed microseisms, at ocean depths of 100 m, to have twice the frequency of the dominant ocean wave. A recent paper by Webb and Cox<sup>10</sup> suggests that some of the seismic noise at periods between 10 and 40 s is a result of pressure disturbances above the sea surface. Their study also indicates that gravity-wave-induced seabed motion dominates seafloor noise above 40-s wave periods. Seafloor noise can also be quite large in the vicinity of ocean-bottom hydrothermal vents as was found by Bibee and Jacobson.<sup>11</sup> This result also

raises the question whether microseisms, at least in part, may be a result of subocean processes.

Several early seismic array studies on land have had a great deal of success in measuring the propagation characteristics of microseisms. The propagation velocities of microseisms found by LaCoss *et al.*<sup>12</sup> and Capon,<sup>13</sup> using data from the large-aperture LASA array in Montana, show microseismic velocities of about 3.5 km/s above 3 s, and a very fast phase velocity of 13.5 km/s at shorter periods. At the longer wave periods, LaCoss *et al.*<sup>12</sup> found the dominant wave energy to be primarily first-mode Rayleigh waves and Love waves. Body waves and higher mode Rayleigh waves were found to be significant at shorter wave periods.

Of current interest in the study of ambient seismic background noise is to understand the propagation characteristics of these signals in the ocean environment. This type of study would require a small-aperture seismic array tuned particularly for short-period microseisms, 1–3 s. This information can help to shed light on the proper generation mechanism(s) for microseisms. One limiting factor in performing array studies in the ocean, however, is the quality of navigation used in determining the geometry of the instruments. Currently available radio-wave navigation systems (LORAN C) are insufficient for array studies requiring positions accurate to within several meters, which is a necessity in order to study the directional spectra of background noise in the ocean. For this reason, along with the fact that many instruments recording contemporaneously are required to

resolve the propagation direction of seismoacoustic energy, experimental data from small-aperture seismic arrays deployed in the ocean are hard to collect.

### I. EXPERIMENT

During the summer of 1987, the Geo-Acoustics Laboratory of the University of Miami conducted an ocean-bottom seismometer (OBS) array experiment on the shallow continental shelf, east of New Jersey. The experiment was designed to measure the directional spectra from seabed motion in the ULF/VLF range, to quantify gravity-wave-coupled seabed motion, and to determine the propagation velocity and spectral characteristics of microseismic noise.

The site location for the directional spectra array study is the Atlantic Generating Site (Fig. 1). This site (39°28'N, 74°15'W, water depth = 12.5 m) is chosen since the upper geologic structure from standard penetration tests of the area to 50-m depth and previous geophysical studies are well known (Dames and Moore<sup>14</sup>; Hathaway *et al.*<sup>15</sup>; Miller and Dill<sup>16</sup>; Stahl<sup>17</sup>; Trevorrow *et al.*<sup>18-20</sup>). A total of six OBSs were successfully deployed; four were plate mounted and two were buried to 0.5-m depths using a water jet burying system. Seismic and pressure channels were tuned to ULF/VLF band, 0.5–100 s. In addition to the standard OBS data channels, the instruments also supported two inclinometer channels to interrogate OBS attitude and an electronic compass. To meet the constraint for shipboard real-time recording, the R/V ATLANTIC TWIN maintained a three-point mooring throughout the experiment.

To determine array geometry, a series of airgun shots were fired from a small launch during calm seas off the starboard and stern of the ship. Distances to the zodiak were measured from a tethered graduated line. A total of 11 starboard shots at 23-m spacings and a gun depth of 9 m, and six stern shots with a gun depth of 11 m were successfully fired. During this phase of the experiment, seismic and pressure

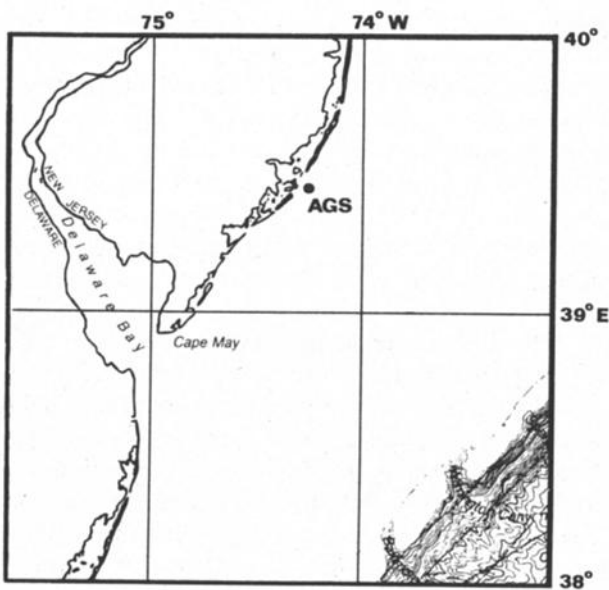


FIG. 1. Atlantic generating site for the directional spectra study [after Ewing and Rabinowitz (Ref. 36)].

TABLE I. Location of instruments determined from nonlinear inversion of refracted sediment arrival times.

Instrument	X	Y	rms error in predicted range (m)
301	299.60 ± 5.6	- 14.21 ± 4.7	3.8
302	64.92 ± 2.6	101.82 ± 1.3	3.0
303	103.52 ± 5.4	329.65 ± 3.3	4.1
304	14.71 ± 1.6	- 170.98 ± 1.7	4.3
305	- 4.95 ± 2.8	- 281.85 ± 2.6	5.2
307	139.89 ± 2.3	- 37.95 ± 2.1	5.7

channels were switched to high-frequency band settings that provide measurable response to 1 kHz. Using the travel time information from these airgun shots having known location, the instrument locations can be found. The method is well known (e.g., Creager and Dorman<sup>21</sup>) and involves nonlinear inversion of travel time data.

An inherent assumption in using travel times to determine locations for close in shots is that the travel path of the first arrival is known. Sediment velocities for the study area average 1700 m/s (Trevorrow *et al.*<sup>20</sup>). Using this information, along with the fact that shot depths were close to the seafloor, suggests that the first arrivals are refracted sediment arrivals and not direct water waves. Before implementation of the inversion method, the data were first corrected to the seafloor using the delay time through a homogenous layer (Purdy<sup>22</sup>; Raitt<sup>23</sup>) for the travel path through the water. The results of applying nonlinear seismic inversion to determine the OBS locations are summarized in Table I and in a map view in Fig. 2. Coordinate uncertainties determined from the covariance of model parameters range from 1.3–5.6 m; rms errors in predicted range are from 3.0–5.7 m.

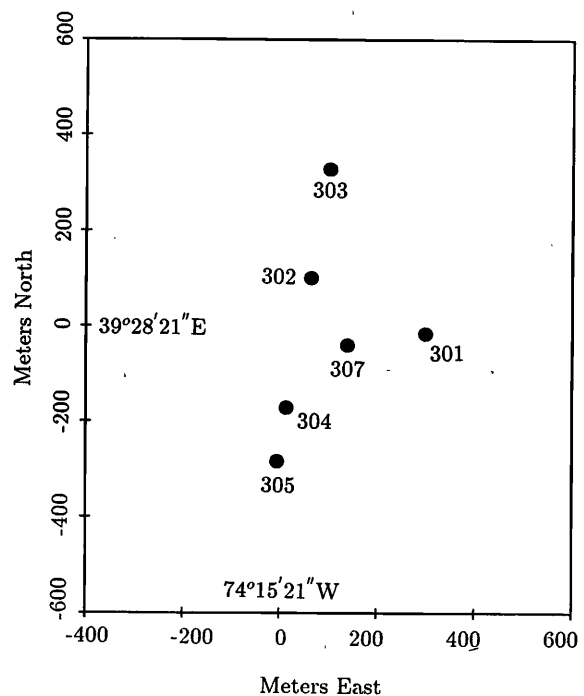


FIG. 2. OBS locations determined from nonlinear seismic inversion of seismic travel times. OBSs 301 and 303 are buried; the rest are deployed on a plate and are unburied.

## II. DIRECTIONAL SPECTRA ANALYSIS

The directional spectral response  $D(k)$  for a plane wave propagating in two dimensions with wavenumber vector  $k$  is given by

$$D(k) = \sum_{ij} R_{ij} \{ \exp^{-i} [k_x(x_i - x_j) + k_y(y_i - y_j)] \}, \quad (1)$$

where  $(x_i, y_i)$  and  $(x_j, y_j)$  are the station coordinates of the  $i$ th and  $j$ th elements in the array. Here,  $R_{ij}$  is the cross spectrum between the  $i$ th and  $j$ th stations:

$$R_{ij} = \overline{S_i S_j^*}, \quad (2)$$

with  $S$  denoting the complex spectrum. The overbar refers to ensemble averaging of the cross spectrum in time and frequency. It is also common in directional spectra analysis to calculate Eq. (1) using normalized cross spectra rather than unnormalized cross spectra, as well as to apply weighting coefficients in the summation (Haubrich<sup>24</sup>). For our particular analysis, however, we choose equal weights for simplicity and unnormalized cross spectra to indicate the true coherent power in the array.

To compute cross spectra, we examine 2.84 h of recorded data beginning on 29 August 1987 at 3:45 p.m. (EST). FFTs are computed using 512 s of data sampled at 4 Hz with a 10% cosine taper. The data are then response corrected. Cross spectra representing a total of 41 ensemble averages for a moving window with 50% overlap are then calculated for both vertical and pressure channels. The data chosen for the analysis are taken during a time when the local ocean-wave state and atmospheric conditions were most statistically stationary.

The application of Eq. (1) to calculate the directional spectra also requires a relation between wavenumber  $k$ , and frequency  $\omega$ . We apply both the water wave dispersion relationship:

$$\omega^2 = gk \tanh(kd), \quad (3)$$

where  $g$  is the gravitational constant,  $d$  is water depth; and the linear relation

$$\omega = kc, \quad (4)$$

where  $c$  is the apparent velocity.

A useful measure for determining the applicability of directional spectra analysis is the normalized cross spectrum function, known as coherence:

$$\gamma^2 = \frac{|\overline{S_i S_j^*}|^2}{|\overline{S_i S_i^*}||\overline{S_j S_j^*}|}. \quad (5)$$

The coherence function  $\gamma^2$  is a real-valued quantity between the values of 0 and 1, 0 signifying that there is no statistical correlation, and 1 signifying a perfect statistical correlation between signals. The statistical basis for application of directional spectra analysis is that there is spatial coherence of wave energy measured across the array. Figures 3–5 are vertical seismometer spatial coherence plots for OBSs 301–307 (range = 161 m), 301–302 (range = 262 m), and 301–304 (range = 325 m) comparisons. At short range (OBS 301–307) and intermediate range (OBS 301–304), two distinct bands of high coherence with relatively stable phase are

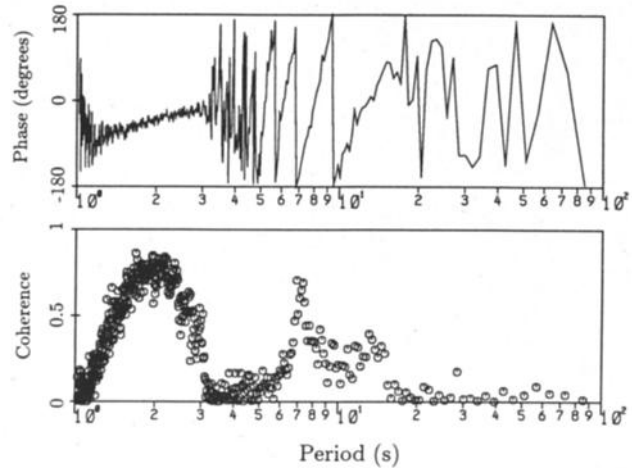


FIG. 3. Coherence and phase between OBS 301 and 307 vertical seismometers (range = 161 m).

identifiable. The band of high coherence centered near 10 s is due to ocean gravity waves. The coherence in this band is highest at short ranges and decreases as the range between spatial comparisons increases. At the longest range (OBS 301–304), the coherence at ocean-wave periods near 10 s is very low. The other well-defined wave-energy band showing high coherence is centered at a period of 2 s and has a 2-s bandwidth. The coherent energy in this band is due to seafloor microseisms propagating across the array.

The microseism and gravity-wave bands are also clearly identified on individual spectra, as in Fig. 6. The seismometers indicate that there are large seafloor motions between 1 and 3 s. All the sensors registered gravity waves for periods above 7 s. A seismoacoustic window appearing between the microseisms and gravity waves, and centered at 4 s, is also shown. This window normally occurs below the cutoff period of gravity-wave pressure disturbances propagating to the seafloor and is thus primarily a function of the water depth.

Spatial coherence plots between pressure sensors for

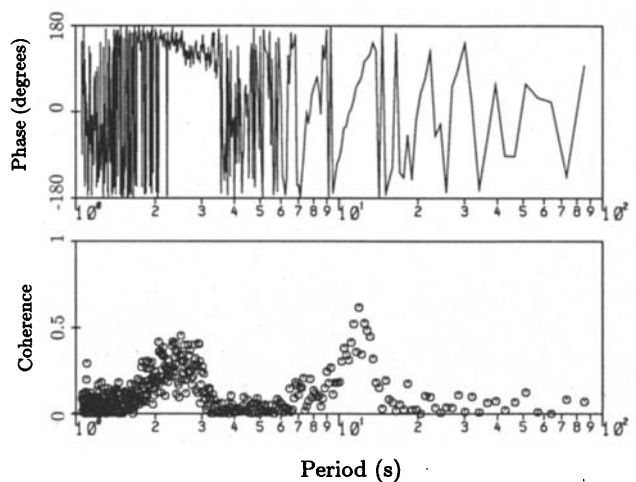


FIG. 4. Coherence and phase between OBS 301 and 302 vertical seismometers (range = 262 m).

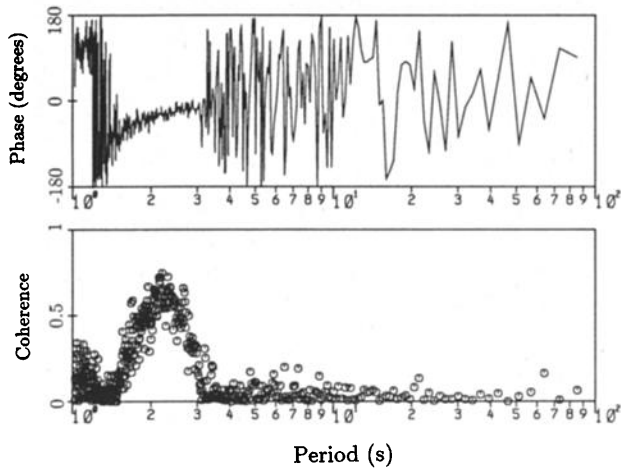


FIG. 5. Coherence and phase between OBS 301 and 304 vertical seismometers (range = 325 m).

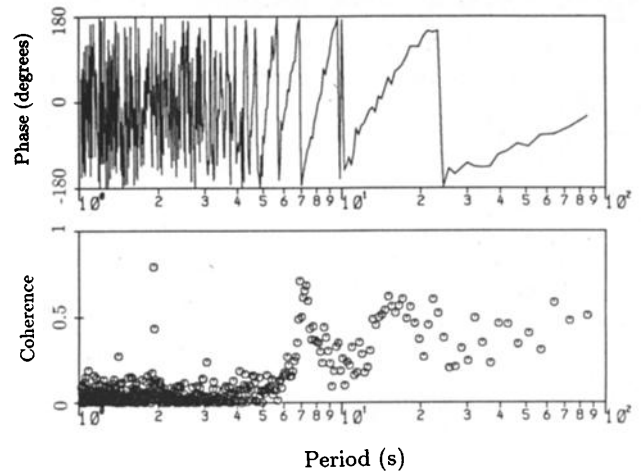


FIG. 7. Coherence and phase between OBS 301 and 307 pressure signals (range = 161 m).

OBS 301–302 and 301–307 comparisons are shown in Figs. 7 and 8. High coherence above 7 s out to long ocean-wave periods of 100 s is present. Vertical seismometer spatial plots show little or no coherence at very long ocean-wave periods.

The directional resolving power of the array is also important to identify for the study undertaken. The beam response for an array of  $m$  elements is

$$B(k, \theta, \theta_0) = 1 + 2 \sum_{n=1}^m \cos [k(x_i - x_j)(\cos \theta - \cos \theta_0) + k(y_i - y_j)(\sin \theta - \sin \theta_0)], \quad (6)$$

where  $\theta_0$  is the array looking angle. Shown in Fig. 9 is  $B$  for wavelengths  $\lambda = 200, 500,$  and  $1000$  m for the NJ87 array. The array beam response shows good resolution as well as sidelobe suppression at these wavelengths.

The coherence function is a time-averaged quantity and can be used to represent the statistical significance of data collected for array processing. Because there are shown to be strong spatial correlations for long-period ocean waves measured by the pressure array, and for microseismic noise measured by the vertical seismometer array, in addition to an array beam response with little sidelobes, directional spectra analysis is appropriate for the seismoacoustic data collected during the New Jersey 1987 OBS array study.

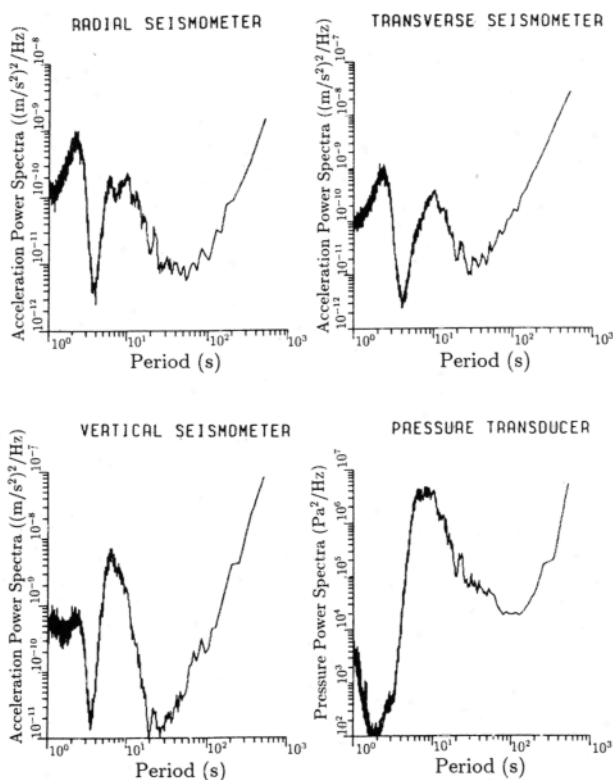


FIG. 6. Averaged power spectrum for pressure and seismic motions measured by buried OBS 301.

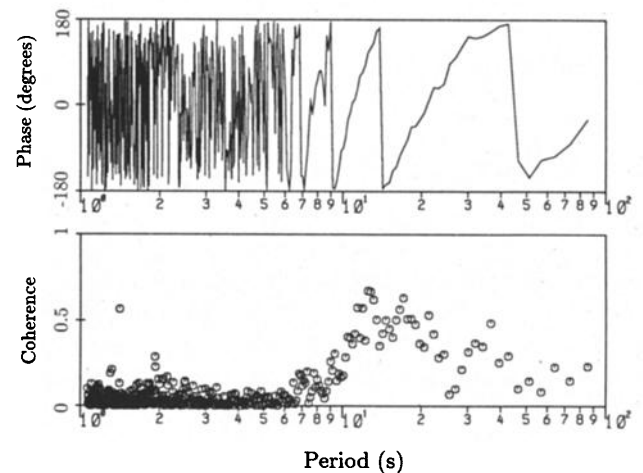


FIG. 8. Coherence and phase between OBS 301 and 302 pressure signals (range = 262 m).

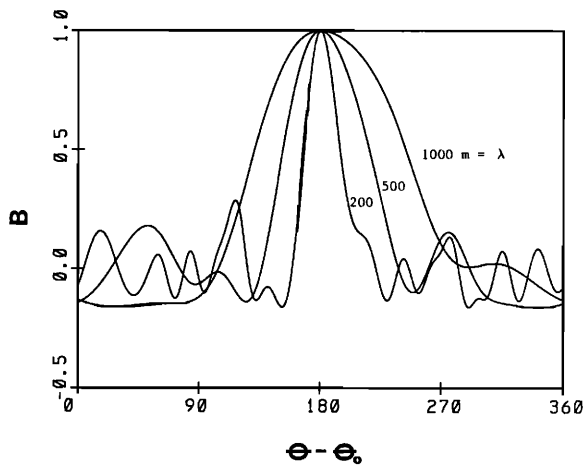


FIG. 9. Beam response of the NJ87 array for various wavelengths. Note that sidelobe responses are very low compared to the primary lobe.

### III. PRESSURE ARRAY RESULTS

Using the water-wave dispersion relation, we compute directional spectra over the period range of 15–85 s using the pressure channel for each OBS. Shown in Figs. 10 and 11 are power (dB) contours representing the response of the array for a particular direction and wave period. The significant wave periods are shown to be wave bands centered at 16 and 24 s (Fig. 10) and 40 and 62 s (Fig. 11). Directionality is less resolved at the shorter periods. The wave direction is much better resolved at larger wavelengths. In Fig. 11, the long-period ocean gravity waves are traveling mostly from the east–southeast (approximately N115E). The peak contours from 15–20 s indicate that gravity waves are traveling almost directly out of the east (approximately N100E). The resolving power of the OBS array below periods of 15-s ocean waves is degraded since the array interelement dimensions

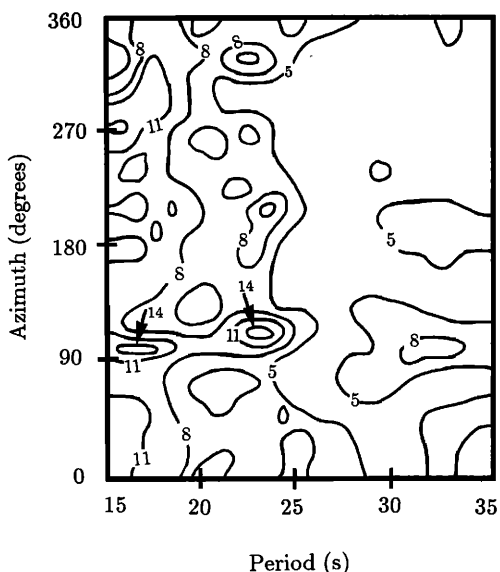


FIG. 10. Directional spectra of intermediate-period ocean waves measured with the pressure array. Contour interval = 3 dB ( $\text{Pa}^2/\text{Hz}$ ).

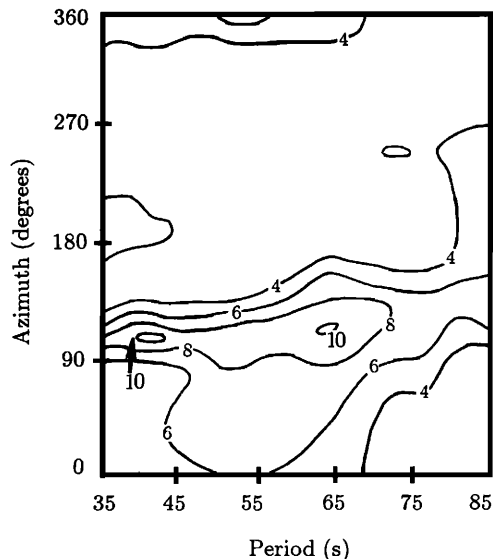


FIG. 11. Directional spectra of long-period ocean gravity waves measured with the pressure array. Contour interval = 2 dB ( $\text{Pa}^2/\text{Hz}$ ).

are larger than the wavelengths of propagating gravity waves. As will be discussed later, particle motion analysis is used to measure propagation directions below 15 s.

### IV. VERTICAL SEISMOMETER ARRAY RESULTS

Applying Eq. (1) to the vertical seismometer data, the directional spectral response of the array in the microseismic band 1.5–2.5 s is calculated. Shown in Fig. 12 are dB contours of integrated array power interrogated for propagation azimuth and phase velocity. The peak response of the array is found at phase velocities near 200 m/s and at an azimuth of N150E. Directional spectral response for phase velocities greater than those shown in Fig. 12 have also been calculated

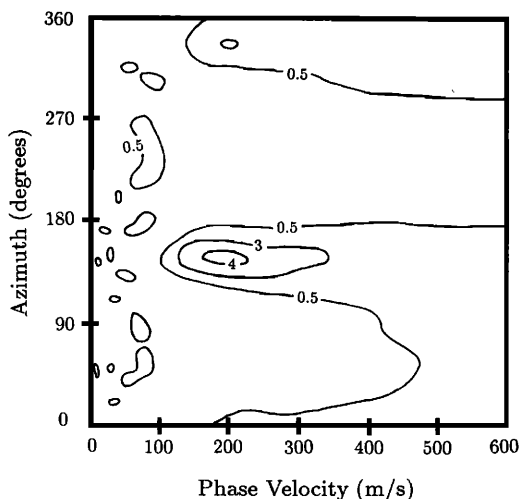


FIG. 12. Directional spectra of microseisms in the period band 1.5–2.5 s measured by the vertical seismometer array. Contours represent relative acceleration squared power ( $\text{m}^2/\text{s}^4/\text{Hz}$ ). Contour interval = 2.5 dB. (Additional contour at 4 dB is added to emphasize peak array response.)

and found to be low. There is a small bimodal response of the array as measured by a secondary peak near  $330^\circ$  and for a phase velocity of 200 m/s.

The uncertainty in the directional spectra shown can be estimated from the uncertainty in the coherence function. The coherence error resulting from finite sampling is

$$\epsilon = \sqrt{2(1 - \gamma^2)} / \gamma \sqrt{n_d} \quad (7)$$

(Bendat and Piersol<sup>125</sup>), where  $n_d$  is the number of ensemble averages times the number of coarray elements. For an average coherence of 0.7 measured in the microseismic band, 41 ensemble averages, and 15 coarray elements, the error  $\epsilon$  is less than 4%. The 95% confidence interval for coherence lies between 0.66 and 0.74. The errors in directional spectra due to finite sampling are thus very small. The total error for directional spectra also contains the uncertainty in instrument location. However, for the wavelengths of interest, which are shown to be approximately 400 m (Fig. 12), a maximum location error of 5 m (Table I) introduces very little additional error.

## V. PARTICLE MOTION ANALYSIS

The direction of seismoacoustic wave energy can also be determined from particle motion studies for a single OBS. If  $X_w$  and  $Y_w$  represent the horizontal east-west and north-south complex amplitude displacement spectra for a given wavenumber, then an estimate of the direction of wave energy  $A_w$  in the first geometric quadrant is given by

$$A_w = \tan^{-1}(|Y_w|/|X_w|). \quad (8)$$

To find whether motion is in the second and fourth quadrants, we examine the phase of the cross spectrum between the horizontal components:

$$\theta_{XY} = \tan^{-1}[\text{Im}(\overline{X_w Y_w^*}) / \text{Re}(\overline{X_w Y_w^*})]. \quad (9)$$

For  $|\theta_{XY}|$  equal to 0, motion is in the first and third quadrants; for  $|\theta_{XY}|$  equal to  $\pi$ , motion is constrained to the second and fourth quadrants. Assuming the wave direction is in the first or fourth quadrants, then the type of particle motion, either retrograde or prograde, can be found by examining the phase of the cross spectrum between the combined horizontal motion and vertical displacement. Letting  $Q_w$  represent the combined horizontal motion in the complex plane,

$$Q_w = X_w + Y_w, \quad (10)$$

and letting  $C_{QZ}$  represent the cross spectrum between combined horizontal and vertical motion  $Z_w$ ,

$$C_{QZ} = \overline{Q_w Z_w^*}. \quad (11)$$

Then, if the phase angle of  $C_{QZ}$  is between 0 and  $-\pi$ , particle motion is prograde in the direction of  $A_w$ . Alternatively, the motion is retrograde (assuming wave is the same direction as  $A_w$ ) if the phase angle of  $C_{QZ}$  is between 0 and  $+\pi$ .

To apply particle motion analysis to determine directional spectra requires a relatively noise-free data set in addition to good coupling between the instrument and the seabed. Directional spectra/particle motion calculations are done for OBS 301, which is a buried instrument. Coupling of this OBS to the seafloor is enhanced and seafloor noise due to

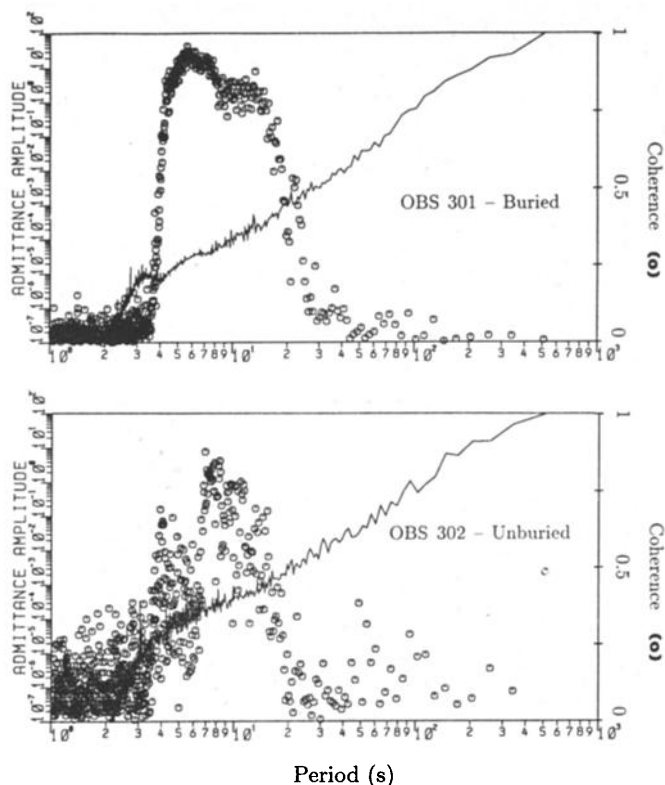


FIG. 13. Noise comparison of horizontal admittance and coherence for buried versus unburied OBSs. Coherence is lower and horizontal admittance is much noisier for the unburied seismometer.

ocean bottom currents is reduced by burying the seismometer housing. Displayed in Fig. 13 is the coherence parameter between pressure and combined horizontal motion for OBS 301 and a plate-mounted OBS, 302. The horizontal coherence parameter defined by

$$\gamma_{QP}^2 = (\gamma_x^2 \overline{X_w X_w^*} + \gamma_y^2 \overline{Y_w Y_w^*}) / (\overline{X_w X_w^*} + \overline{Y_w Y_w^*}), \quad (12)$$

where

$$\gamma_x^2 = |\overline{X_w P_w^*}|^2 / |\overline{X_w}| |\overline{P_w}| \quad (13)$$

and

$$\gamma_y^2 = |\overline{Y_w P_w^*}|^2 / |\overline{Y_w}| |\overline{P_w}|, \quad (14)$$

with  $P_w$  representing the pressure spectrum, has values between 1 and 0, and relates the degree to which the pressure and combined horizontal signal are correlated. The coherence parameter between pressure and horizontal (Fig. 13) is shown to be higher and less noisy for the buried instrument as compared to the unburied instrument. In addition, the admittance between pressure and horizontal components, given by

$$e(w) = \frac{\rho g}{w^2 \cosh(kd)} \sqrt{\frac{(|X_w|^4 + |Y_w|^4)^{0.5}}{|P_w|^2}} \quad (15)$$

(Trevorrow *et al.*<sup>19</sup>), where  $\rho$  is water density, is much noisier for the unburied unit. An important comparison between the two admittance curves shows the buried unit to have an admittance value that is approximately 14 dB less than the unburied unit in the region of high coherence. Ad-

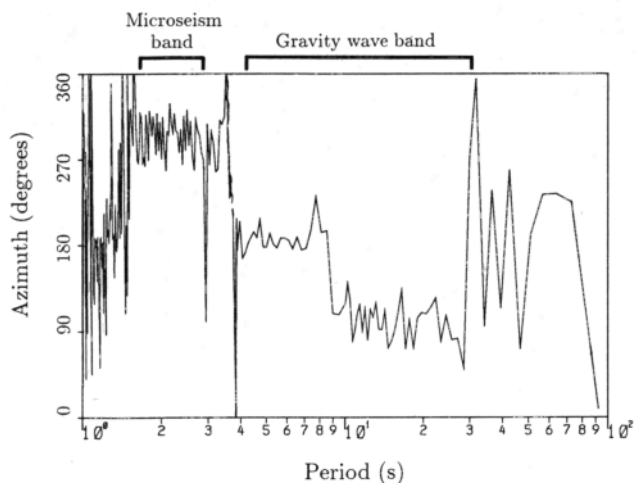


FIG. 14. Directional spectra determined from buried OBS 301 using particle motion analysis. Azimuths shown assume motion is prograde in the direction of propagation.

mittance, which is essentially the transfer function between pressure and horizontal seafloor motion, should show better coherence for larger horizontal signal amplitude. This, however, is not what is observed and indicates that a buried instrument has better coupling to gravity surface waves, in addition to having a lower noise amplitude.

Using particle motion data for buried OBS 301, the azimuth  $A_w$  is calculated (Fig. 14). A three-frequency bin average was applied below 10 s. Two distinct azimuths in the gravity-wave band are apparent between long-period (12–30 s) and short-period gravity waves (5–9 s). If one reexamines the pressure coherence plot for the close-range spatial comparison (Fig. 7), two distinct regions of high coherence between short- and long-period gravity waves are apparent above and below 10 s. This is also evidenced by a small double peak in the combined horizontal and pressure coherence (Fig. 13). The short-range vertical seismometer coherence (Fig. 3) also shows two distinct regions of coupling to ocean gravity waves. These observations are consistent with the two azimuth calculation for gravity waves found from particle motion.

In the microseismic band, if we assume prograde particle motion, Fig. 14 indicates a direction of wave travel out of the west, and an easterly direction of travel assuming retrograde particle motion.

## VI. DISCUSSIONS OF RESULTS

Directional spectra analysis for both pressure and vertical accelerometer data indicate that there are two primary sources contributing to seabed motion: gravity-wave coupling and slow-moving seismic waves. Gravity-wave coupling is the dominant source of seabed motion at 7–30 s wave periods. Alternatively, at short periods below the cutoff period for ocean-wave seafloor pressure disturbances, slow-moving seismic waves are dominant. Rauch<sup>26</sup> has also found low phase velocities for Scholte modes generated via active sources.

From particle motion studies it is determined that short-period, 1.5–2.5 s microseisms have either prograde motion

out of the northwest or retrograde motion for a wave traveling from the southeast. Because a northwestern origin for these waves is unlikely, as is indicated by the vertical seismometer array study (Fig. 12), the microseisms in this band most likely have retrograde particle motion. Subseismic phase velocities for waves exhibiting retrograde particle motion at the seafloor would be indicative of Scholte-type interface waves (Rauch<sup>26</sup>). Given that the microseisms have retrograde motion, then the directions predicted by the vertical seismometer array (Fig. 12) and the independent measurement from particle motion (Fig. 14) agree to within about 20 deg of each other. Since the orientation of the individual sensors for a single instrument are measured using an internal magnetic compass, any changes in the local magnetic declination could account for the small difference in predicted direction from particle motion analysis.

In comparing the direction of travel of long-period gravity waves from particle motion analysis (Fig. 14) and the pressure array directional spectra (Fig. 11), we find a good correspondence in the measured propagation direction. The measured propagation directions between long-period gravity waves (15–85 s) and short-period gravity waves (5–9 s) are shown to be perpendicular to one another. The direction of travel of the short-period waves is consistent with the local wind direction which was out of the south. The long-period waves, which are less inclined to respond to local wind conditions, are from the east and are due to storms at sea.

An inherent assumption in our interpretation of particle motion data is that the microseisms are principally vertically polarized interface waves (Stacey<sup>27</sup>). The existence of Love waves would significantly alter the directional spectra calculated and would negate the simplified particle motion study undertaken. However, azimuths determined in the microseismic (as well as gravity wave) band are relatively stable and are a good indication that vertically polarized seafloor motion dominates horizontally polarized seafloor motions for our particular data set.

The measured phase velocities for the microseisms are appropriate, given the available geophysical data for the study area. Shown in Fig. 15 is the seismic profile measured down to 50 m at AGS using the bottom shear modulus profiler (BSMP) method of Yamamoto and Torii.<sup>28</sup> The average shear-wave velocity over the profile is 340 m/s. The Scholte wave would be slower than a free-surface Rayleigh wave, which, in turn, would be slower than a shear wave. The seismic profile measured to 50 m would only correspond to about a quarter-wavelength for those wavelengths measured by the OBS array. The Scholte-wave phase velocities measured are probably close to the “natural” phase velocity that would be measured if this interface wave mode were excited through the observed seismic structure. Future research plans will include modeling of the Scholte-wave mode through an extended version of the seismic structure currently known for the Atlantic Generating Site, using normal-mode propagation techniques (e.g., Badley and Yamamoto<sup>29</sup>).

Previous investigators (Munk *et al.*<sup>30</sup>; Bowen and Guza<sup>31</sup>; Guza and Thornton<sup>32</sup>) have found long shore propagation at periods of 20–200 s to be a dominant type of wave

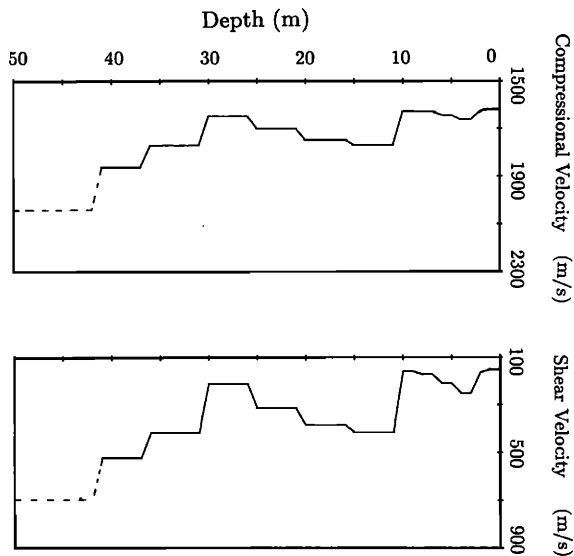


FIG. 15. Shallow seismic structure for the Atlantic generating site. The average shear velocity through the first 50 m is 340 m/s.

propagation in the near coastal region. Long shore waves, commonly referred to as the infragravity edge waves (Shay and Guza<sup>33</sup>), are thought to be shallow-water gravity waves that are trapped in the nearshore (Gallagher<sup>34</sup>). Most of the experiments up to date, however, have clearly identified the existence of edge waves within 500 m of the shoreline. The array study from our experiment conducted at the Atlantic Generating Site, 6 km offshore, indicates cross-shore propagation of infragravity waves. The existence of edge waves at these offshore ranges has not been clearly quantified. Gallagher<sup>34</sup> suggests the edge-wave energy falls off as  $e^{-2kx}$  away from the shore. At a 6-km distance compared to a measurement made 0.5 km offshore, a 22-dB decrease in edge-wave power would result. Furthermore, the New Jersey coastline in the vicinity of the experiment site (see Fig. 1) has numerous inlets which may impede and disperse near coastal edge waves, and thereby make them undetectable by an array of sensors.

Alternatively, in the paradigm of Longuet-Higgins and Stewart,<sup>35</sup> waves of infragravity wave periods are generated by nonlinear waves having the same wavelength and period of the first-order wave group. These long-period gravity waves can travel from the seaward direction as they are generated by the wind in the coastal zone (Gallagher<sup>34</sup>) and can be reflected seaward as a free wave known as a "leaky"-wave mode (Longuet-Higgins<sup>35</sup>). Our array study conducted 6 km offshore confirms onshore propagation of infragravity waves. The leaky-wave mode, which would be indicative of a reflected onshore infragravity wave, is definitely not registered by the array. Again, this may be a result of the offshore distance to the array, as well as the complicated coastal structure at the closest point of approach to the array that might diminish reflected wave energy.

An interesting observation is that the microseisms are traveling in a direction midway between long- and short-period gravity waves. Longuet-Higgins<sup>1</sup> suggests that microseisms can be generated by waves of similar period traveling in opposite directions. Directional spectra analysis from

our study shows no bimodal array response to either long- or short-period ocean gravity waves.

## VII. CONCLUSIONS

The conclusions based on analysis of the New Jersey 1987 OBS array data are the following: (1) Gravity-wave-coupled seabed motion in shallow coastal waters is dominant at long periods, 5–100 s. (2) Seabed motion at short periods, 1–3 s, is primarily a result of seismic waves traveling at apparent velocities close to 200 m/s. Microseismic propagation velocities in the ocean are an order of magnitude less than for microseisms found on land at similar wave periods. (3) Particle motion at 1–3 s is retrograde. This suggests that seafloor microseisms are due to Scholte interface waves at these short periods.

Additional seismoacoustic measurements at nearer and at larger offshore ranges, as well as for different array spacings, are required to substantiate the findings in this study. Measurements at various array sizes will help to identify the continuity of spatial coherence of microseisms. Array measurements over varying sea states will also help to correlate microseism propagation and excitation dependence on gravity-wave directional spectra.

## ACKNOWLEDGMENTS

This work was supported under ONR code 1125 OA with the guidance and support of Dr. Marshall Orr and Dr. Raymond Fitzgerald. We would also like to thank the Captain and crew of the R/V ATLANTIC TWIN for helping with the ocean-going data acquisition.

- <sup>1</sup>M. S. Longuet-Higgins, "A Theory of the Origin of Microseisms," *Philos. Trans. R. Soc. London, Ser. A* **243**, 1–35 (1950).
- <sup>2</sup>K. A. Hasselmann, "A Statistical Analysis of the Generation of Microseisms," *Rev. Geophys.* **1**, 177–210 (1963).
- <sup>3</sup>V. H. Goerke and M. W. Woodward, "Infrasound Observation of a Severe Weather System," *Mon. Weather Rev.* **94**, 395–398 (1966).
- <sup>4</sup>G. G. Sorrells and E. J. Douze, "A Preliminary Report on Infrasonic Waves as a Source of Long-Period Seismic Noise," *J. Geophys. Res.* **79**, 4908–4917 (1974).
- <sup>5</sup>G. G. Sorrells, "A Preliminary Investigation into the Relationship between Long-Period Seismic Noise and Local Fluctuations in the Atmospheric Pressure Field," *Geophys. J. R. Astron. Soc.* **26**, 71–82 (1971).
- <sup>6</sup>B. Gutenberg, "Microseisms, Microbaroms, Storms, and Waves in Western North America," *Trans. Am. Geophys. Union* **34**, 161–173 (1953).
- <sup>7</sup>M. Ewing and F. Press, "Further Study of Atmospheric Pressure Fluctuations Recorded on Seismographs," *Trans. Am. Geophys. Union* **34**, 95–100 (1953).
- <sup>8</sup>R. A. Haubrich, W. H. Munk, and F. E. Snodgrass, "Comparative Spectra of Microseisms and Swell," *Bull. Seismol. Soc. Am.* **53**, 27–37 (1963).
- <sup>9</sup>A. C. Kibblewhite and K. C. Ewins, "Wave-Wave Interactions Microseisms and Infrasonic Ambient Noise in the Ocean," *J. Acoust. Soc. Am.* **78**, 981–995 (1985).
- <sup>10</sup>S. C. Webb and C. S. Cox, "Observation and Modeling of Seafloor Microseisms," *J. Geophys. Res.* **91**, 7343–7358 (1986).
- <sup>11</sup>L. D. Bibee and R. S. Jacobson, "Acoustic Noise Measurements on Axial Seamount, Juan de Fuca Ridge," *Rev. Geophys. Res. Lett.* **13**(9), 957–960 (1986).
- <sup>12</sup>R. T. LaCoss, E. J. Kelly, and M. N. Toksoz, "Estimation of Seismic Noise Structure using Arrays," *Geophysics* **34**, 21–38 (1969).
- <sup>13</sup>J. Capon, "Long-Period Signal Processing Results for the Large Aperture Seismic Array," *Geophysics* **33**, 452–472 (1969).
- <sup>14</sup>Dames and Moore Company Ltd., "Supplementary Subsurface Investigation: Vibracore Program, Atlantic Generating Station," for the Public

- Service Electric and Gas Company, Granford, NJ (1974).
- <sup>15</sup>J. C. Hathaway, J. S. Schlee, C. W. Poag, P. C. Valentine, E. G. A. Weed, M. H. Bothar, F. A. Kohout, F. T. Manheim, R. Schoen, R. E. Miller, and D. M. Schulte, "Preliminary Summary of the 1976 Atlantic Margin Coring Project," United States Geological Survey, Open File Rep. No. 76-844 (1976), p. 217.
- <sup>16</sup>H. J. Miller and C. Dill, "Final Report, Geophysical Investigation of Atlantic Generating Station Site and Offshore Region," for the Public Service Electric and Gas Company, Newark, NJ (1974).
- <sup>17</sup>L. Stahl, J. Koczan, and D. Swift, "Anatomy of a Shoreface-connected Sand Ridge on the New Jersey Shelf: Implications for the Genesis of the Shelf Surficial Sand Sheet," *Geology* **2**, 117-120 (1974).
- <sup>18</sup>M. Trevorrow, T. Yamamoto, A. Turgut, C. Abbott, M. Badiy, D. Goodman, and K. Ando, "High Resolution Bottom Shear Modulus Profiler Experiments on the New Jersey Shelf, Summer 1987," RSMAS Tech. Rep. 88-002, University of Miami (1988).
- <sup>19</sup>M. Trevorrow, T. Yamamoto, M. Badiy, A. Turgut, and C. Conner, "Experimental Verification of Seabed Shear Modulus Profile Inversions using Surface Gravity (Water) Wave-Induced Seabed Motion," *Geophys. J. R. Astron. Soc.* **93**, 419-436 (1988).
- <sup>20</sup>M. V. Trevorrow, M. Badiy, A. Turgut, C. S. Conner, and T. Yamamoto, "A Quantitative Analysis of Seabed Shear Modulus Inversions from Experiments on the New Jersey Shelf in August, 1986," RSMAS TR-87-003, Gal Rep. 1003, University of Miami (1987).
- <sup>21</sup>K. C. Creager and L. M. Dorman, "Location of Instruments on the Seafloor by Joint Adjustment of Instrument and Ship Positions," *J. Geophys. Res.* **87**, 8379-8388 (1982).
- <sup>22</sup>G. M. Purdy, "The Correction for the Travel Time Effects of Seafloor Topography in the Interpretation of Marine Seismic Data," *J. Geophys. Res.* **87**, 8389-8396 (1982).
- <sup>23</sup>R. W. Raitt, G. G. Shor, Jr., T. J. G. Francis, and G. B. Morris, "Anisotropy of the Pacific Upper Mantle," *J. Geophys. Res.* **74**, 3095-3109 (1969).
- <sup>24</sup>R. A. Haubrich and K. McCamy, "Microseisms: Coastal and Pelagic Sources," *Rev. Geophys.* **7**, 539-571 (1969).
- <sup>25</sup>J. S. Bendat and A. G. Piersol, *Random Data, Analysis and Measurement Procedures*, 2nd ed. (Wiley, New York, 1986), p. 310.
- <sup>26</sup>D. Rauch, "Experimental and Theoretical studies of Seismic Interface Waves in Coastal Waters," in *Bottom Interacting Ocean Acoustics*, edited by W. Kuperman and F. B. Jensen (Plenum, New York, 1980), pp. 307-327.
- <sup>27</sup>F. D. Stacey, *Physics of the Earth*, 2nd ed. (Wiley, New York, 1977), p. 141.
- <sup>28</sup>T. Yamamoto and T. Torii, "Seabed Shear Modulus Profile Inversion Using Surface Gravity (Water) Wave-Induced Bottom Motion," *Geophys. J. R. Astron. Soc.* **85**, 413-431 (1986).
- <sup>29</sup>M. Badiy and T. Yamamoto, "Acoustic Normal Modes in a Homogeneous Ocean Overlaying Layered Anisotropic Porous Beds," *J. Acoust. Soc. Am.* **77**, 954-961 (1985).
- <sup>30</sup>W. Munk, F. Snodgrass, and F. Gilbert, "Long Waves on the Continental Shelf: An Experiment to Separate Trapped and Leaky Modes," *J. Fluid Mech.* **13**, 481-504 (1964).
- <sup>31</sup>A. J. Bowen and R. T. Guza, "Edge Waves and Surf Beat," *J. Geophys. Res.* **83**, 1913-1920 (1978).
- <sup>32</sup>R. T. Guza and E. B. Thornton, "Observations of Surf Beat," *J. Geophys. Res.* **90**, 3161-3172 (1985).
- <sup>33</sup>J. O. Shay and R. T. Guza, "Infragravity Edge Wave Observations on Two California Beaches," *J. Phys. Oceanogr.* **17**, 644-663 (1987).
- <sup>34</sup>R. T. Gallagher, "Generation of Surf Beat by Nonlinear Wave Interactions," *J. Fluid Mech.* **49**, 1-20 (1971).
- <sup>35</sup>M. S. Longuet-Higgins and R. W. Stewart, "Radiation Stress and Mass Transport in Gravity Waves, with Application to 'Surf Beats'," *J. Fluid Mech.* **13**, 481-504 (1962).
- <sup>36</sup>J. I. Ewing and P. D. Rabinowitz, "Eastern North American Continental Margin and Adjacent Ocean Floor 34°-41°N and 68°-78°W," *Ocean Margin Drilling Program*, Woods Hole, MA (1984).